ISSN 1070-4272, Russian Journal of Applied Chemistry, 2016, Vol. 89, No. 12, pp. 2008−2015. © Pleiades Publishing, Ltd., 2016.

VARIOUS TECHNOLOGICAL PROCESSES

Electrospinning Fabrication of Mesoporous Nano Fe_2O_3-TiO_2@Activated Carbon Fiber Membrane for Hybrid Removal of Phenol from Waste Water[1]

Han Chong, Jing Maoxiang*, Shen Xiangqian, and Qiao Guanjun**

[a] *School of Materials Science and Engineering, Jiangsu University, Zhenjiang, 212013 China*
[b] *Jingjiang College, Jiangsu University, Zhenjiang, 212013 China*
*e-mail: *mxjing2004@ ujs.edu.cn, **gjqiao@mail.ujs.edu.cn*

Received November 24, 2016

Abstract—A mesoporous iron–titanium mixed-oxides@activated carbon(AC) fiber membrane was fabricated by an electrospinning method and applied to the treatment of phenol waste water. The physical and chemical properties of the composite fiber membrane were characterized by powder X-ray diffraction (XRD), scanning electron microscopy (SEM), transmission electron microscopy (TEM), N_2 adsorption/desorption, UV–Vis light diffuse reflectance spectroscopy (DRS), Raman spectroscopy, respectively. The results indicate that the composite nanofiber membrane is composed of α-Fe_2O_3, anatase TiO_2 and activated carbon phases with a specific surface area of 231 m^2 g^{-1} and narrow pore size distribution of 3–6 nm. DRS reveals that the composite membrane has high photons absorption from both ultraviolet light and visible light irradiation owing to the combination of Fe_2O_3, TiO_2 and carbon. The prepared nano Fe_2O_3–TiO_2@AC fiber membrane can act as an efficient reusable photocatalyst and adsorbent for 100% remo val of phenol pollutant. This hybrid technique is hopeful to be widely used in the treatment of various organic waste waters.

DOI: 10.1134/S1070427216120120

INTRODUCTION

Phenol is widely used in industrial and environmental photo-chemistry as well as biological systems due to its important roles as antioxidants and polymer photo-sensitizers [1]. However, phenol is also considered to be a great threat to the environment as its contamination in water at few ppm level is highly carcinogenic to humans and animals [2]. Although many techniques have been implemented for removal and degradation of phenol and phenolic compounds in waste water [3], such as adsorption, biodegradation, membrane extractio n and oxidation, etc., there is still a great challenge to develop a high efficient, low cost technique for removal of various content phenol waste waters.

The heterogeneous photocatalytic process has been proved to be effective for removal of phenol and phenolic compounds [3, 4]. However, the photocatalysis technique is still in the developing stage due to several basic inherited problems, such as long term reaction time, low photonic efficienc y and difficulty to recycle, etc., have not been solved [5, 6]. Recently, more and more catalytic nanomaterials are being developed and utilized in photocatalysis [7]. For example, Ag/TiO_2 [8], Fe/TiO_2 [9, 10], Fe_2O_3 [11], etc. Especially, nano α-Fe_2O_3 as an n-type semiconductor with narrow band gap (2.2 eV) is used as a visible- light excited photocatalyst [11]. However, for mono-component α-Fe_2O_3 material, the high recombination rate of photogenerated electrons and holes hinders its widespread application in photocatalysis. Coupling α-Fe_2O_3 with other semiconductors, such as ZnO, TiO_2, and SnO_2 to form a mixed photocatalyst is proved to be able to enhance the photocatalytic activities [12–14]. This kind of composite photocatalyst could accelerate

[1] The text was submitted by the authors in English.

the separation rate of charge carries in photocatalytic process. Recently, many researchers have prepared the Fe_2O_3/TiO_2 nanocomposite photocatalyst, which can absorb photons from both ultraviolet and visible light because of the different band gaps[15–18].

Although nano-sized composites have high photocatalytic capacity, they face another problem that they are too small to be separated from the slurries when the treatment finished. To solve the problem, a media can be used to support the nanoparticles in order that they can be separated from the water [19, 20]. Activated carbon fiber (ACF) is widely applied in the purification of air and water owing to its higher adsorption capacities than granular activated carbons [21–23]. It can remove both natural organics and various synthetic organic contaminates such as synthetic organic dyes, trichloroethene and phenol, etc. And ACF has great mechanical and physical properties and stability in different chemical and physical conditions, therefore, it can be used as a support of the nanoparticles for water treatment, and solve the separation problem of the nanoparticles [24–26]. Concerning their preparation processes, electrospinning has been regarded as a facile method to prepare polymer fibers or other composite fibers with high specific surface area and porosity, which is also very helpful to fabricate ACF-supported composite photocatalysts.

In this work, a mesoporous nano Fe_2O_3–TiO_2@ activated carbon fiber (ACF) membrane was prepared by an electrospinning method. This kind of composite fiber membrane with interconnected pores, high porosity and large surface area was utilized to treat phenol waste water with the expectation of combining high adsorption capacity of ACFs and high photocatalytic activity of Fe_2O_3/TiO_2 composites.

EXPERIMENTAL

The mesoporous Fe_2O_3–TiO_2@activated carbon nanofiber membranes were fabricated by an electrospinning process followed by a calcination treatment. Specifically, 1.0 g Ferric nitrate ($Fe(NO_3)_3 \cdot 9H_2O$) and 2.0g tetrabutyl titanate ($C1_6H_{36}O_4Ti$) were added to 5.0 g *N,N*-dimethylformamide (DMF) orderly and stirred for 10min to obtain a homogeneous solution A. Meanwhile, 4.0 g polyacrylonitrile (PAN) powders were dissolved in 30.0 g DMF and stirred for 1h to form solution B. Then, the solution A was slowly dropped into solution B with violently mechanical stirring to get a homogeneous viscous solution for electrospinning. The mixed solution was put into a plastic syringe, which is connected with a steel needle of 0.6 mm in internal diameter. A steel roller was placed 20 cm below the needle tip as a receiver to collect the precursor fibers . A voltage of 25 kV was applied on the needle tip to electrospin the solution with a feeding speed of 1.2 mL h^{-1}. The receiver was fixed with a rotating speed of 200 rpm. Second, the precursor fibers were collected, and stabilized at 280°C for 4 h in air. Then the stabilized fiber membranes were pressed between two graphite plates of 1 cm in thickness, heated to 700–800°C with the heating rate of 2°C min^{-1} for holding time of 5–10 h in N_2 atmosphere. When cooled to room temperature, the flexible mesoporous Fe_2O_3–TiO_2@ activated carbon nanofiber membranes were obtained.

The crystal structure of the resulted fibers was determined by an Rigaku 2500 X-ray diffractometer (XRD). The morphology and microstructure of the samples were observed b y a JSM-5600LV scanning electron microscope (SEM) and a JEM2010 transmission electron microscopy (TEM). The specific surface area, pore volume and pore size distribution using the BET technique under N_2 gas were evaluated using NOVA2000 gas sorption analyzer system. X-ray photoelectric spectroscopy (XPS) analysis of the fiber membrane was carried out by an ESCALAB MarkII spectrophotometer, an AlK_α X-ray source was used for the excitation of electrons. UV-vis diffuse reflectance spectra (DRS) of the photocatalysts used to characterize the light absorption band edge were recorded by using a PGENERAL TU-1901 UV-Vis spectrophotometer with pure $BaSO_4$ as a reference. The removal efficiency of phenol was assessed by a free penetration method in a transparent filtrator. In a cycle, 50 mL phenol solution with a content of 20 mg L^{-1} was dropped slowly through the membrane under the irradiation of 500 W simulated visible light. The fiber membrane size is 4.5 cm in diameter and 120 μm in thickness. The UV-Vis absorption spectra of the phenol solutions were obtained using a P GENERAL TU-1901 UV-Vis scanning spectrophotometer in the wavelength range 200–800 nm.

RESULTS AND DISCUSS ION

Figure 1 shows the digital picture of the precursor membrane and the SEM images of the fibers calcined at different conditions. It can be seen that the precursor membrane has a smooth and uniform morphology as

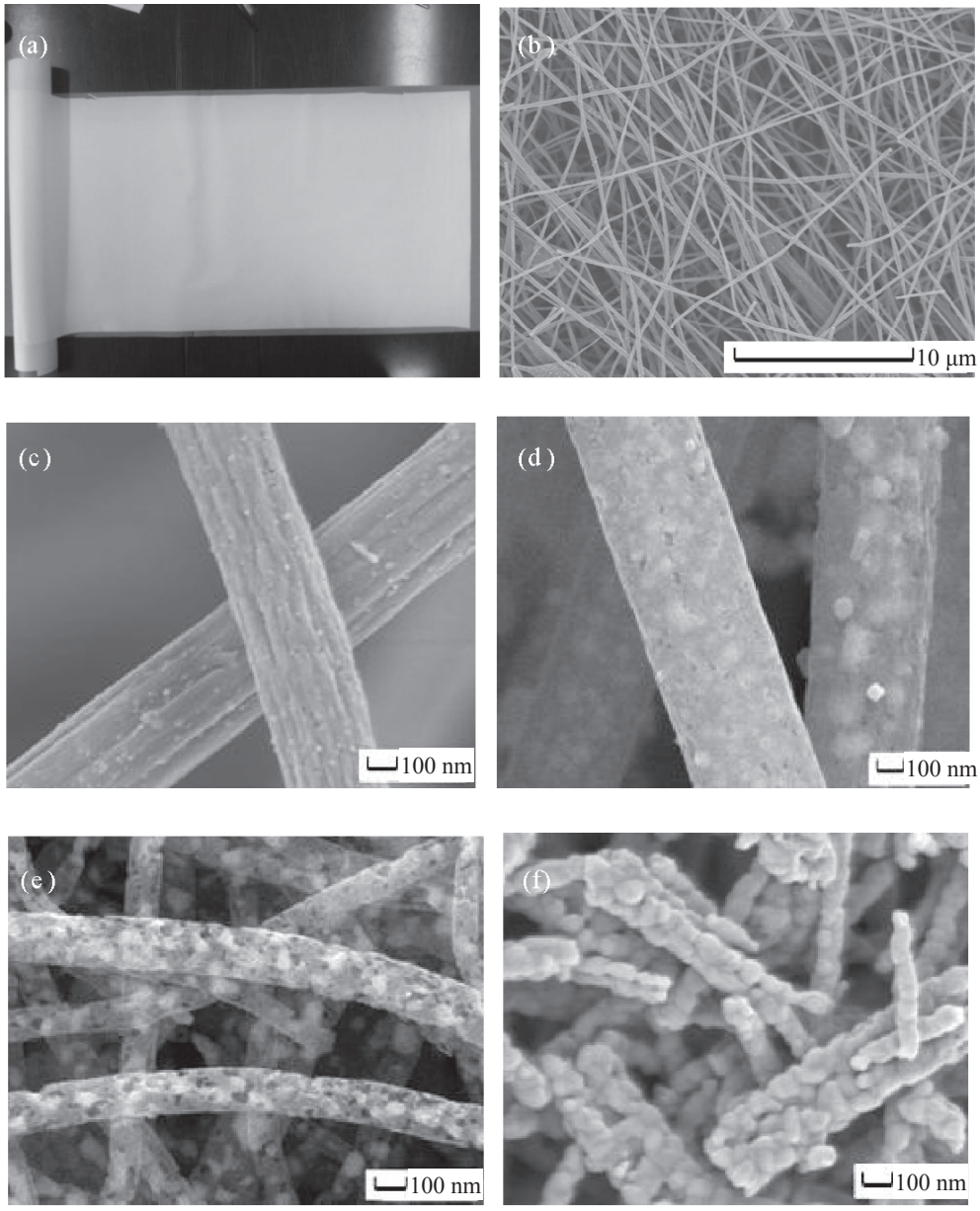

Fig. 1. (a) Digital picture of the precursor membrane and (b–f) SEM images of the fibers calcined at different conditions, (b, c) 700°C 5 h, (d) 700°C 10 h, (e) 750°C 5 h, (f) 800°C 5 h.

a paper, meaning that the electrospinning process is a suitable method to prepare a nanofiber membrane. After calcination at different temperature and holding time, the fiber membrane is not destroyed, still remains a very uniform structure as shown in Fig. 1b with a mean thickness of 120 μm. However, from the high magnification images, it can be observed that the fibers have different morphology and structure. At 700°C for 5 h or 10 h, the surface of the fibers basically keeps smooth and imporous but some particles can be seen indistinctly. With the increase of temperature, these fibers are transformed to porous and with distinct particles. But, when the temperature increased to 800°C, the membrane was destroyed to be short fibers composed with large particles.

Figure 2 shows the XRD patterns of the fiber membrane after calcination at different conditions. From the patterns, different diffraction peaks can be observed with different temperature and holding time, the pattern at 700°C for 5 h just shows a bread peak corresponding

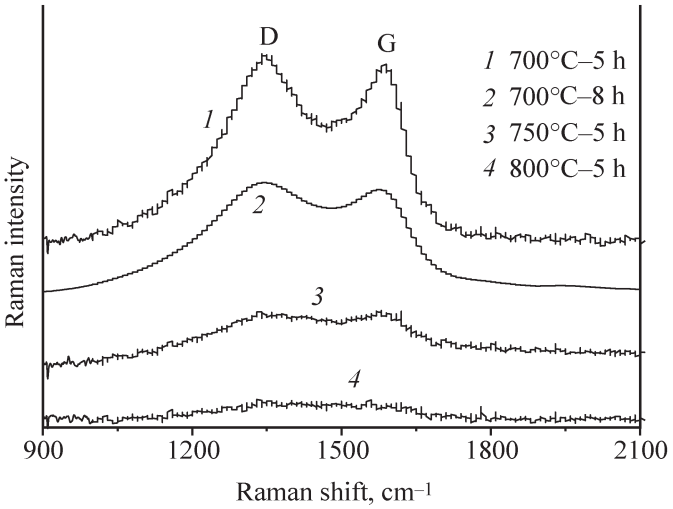

Fig. 2. XRD patterns of the fiber membranes after calcination at different conditions.

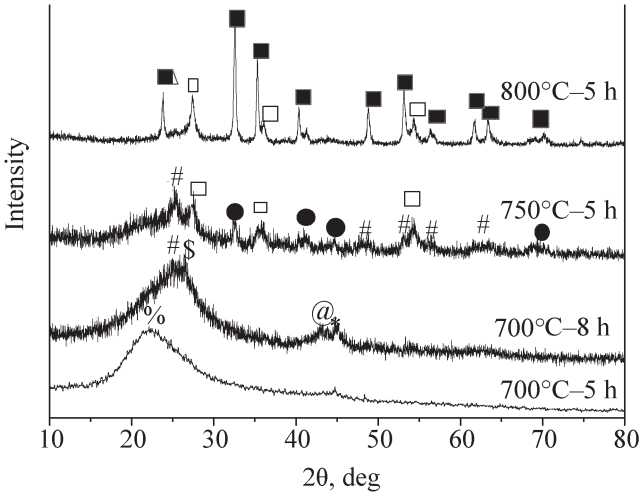

Fig. 3. Raman patterns of the fiber membrane calcinated at different conditions. (■) $FeTiO_3$, (□) R-TiO_2, (#) A-TiO_2, (●) Fe_2O_3, (@) Fe_3C, (*) Fe, ($) Graphite, (%) C.

to the amorphous carbon (PDF#50-0926). When the holding time extends to 8 h, there appears α-Fe peak (PDF#06-0696), anatase TiO_2 peak (P DF#21-1272), amorphous carbon and graphite-2H peak (PDF#50-0926), but a little Fe_3C impure phase (PDF#65-0393) is also detected. When the temperature increases to 750°C and holds for 5 h, the aimed phases of anatase TiO_2, α-Fe_2O_3 (PDF#16-0653) and carbon are all detected, meanwhile, some weak rutile TiO_2 (PDF#65-0191) peaks are also found, which would be beneficial for the activity enhancement of anatase TiO_2 just as the commercial product of Degussa P25 [27]. Continuing increas ing the temperature to 800°C , the anatase TiO_2 and Fe_2O_3 phases are transformed to Fe(II) TiO_3 (PDF#29-0733) and rutile TiO_2.

It is notable that the carbon peak at 2θ = 22.6° is weakened gradually with the increase of calcination temperature, meaning that the content of carbon was reduced accordingly, which can be proved by the SEM images with different morphology and the weakening peak intensity of Raman spectra in Fig. 3. Raman spectra can also provide some surface information about the fibers. Figure 3 shows the Raman spectra of the fiber membrane calcinated at different conditions. It can be observed that all the fibers present a D peak at 1345 cm^{-1} and a G peak at 1582 cm^{-1}, corresponding to disordered carbon and graphitic carbon, respectively, which indicates this carbon in fibers is a kind of activated carbon. Meanwhile, the ratio of I_D/I_G is reduced from 1.06 to 1.0 as the temperature increases from 700°C to 800°C, indicating that the disordered carbon is gradually transformed to graphitic carbon. Therefore, according to the above results, the applicable heat treatment condition is 750°C for 5 h.

To further study the microstructure of the composite fibers, a typical TEM image for the sample calcinated at 750°C for 5 h is shown in Fig. 4. It can be seen that the

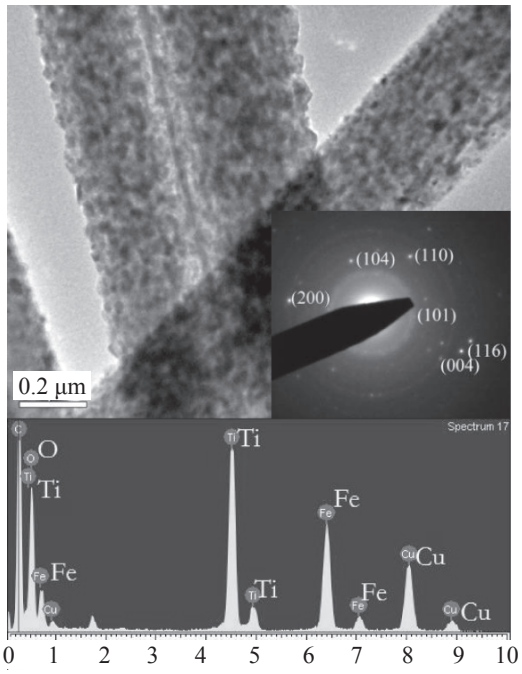

Fig. 4. TEM images and EDS of the fibers calcinated at 750°C for 5 h, the inset is the corresponding SAED of fibers.

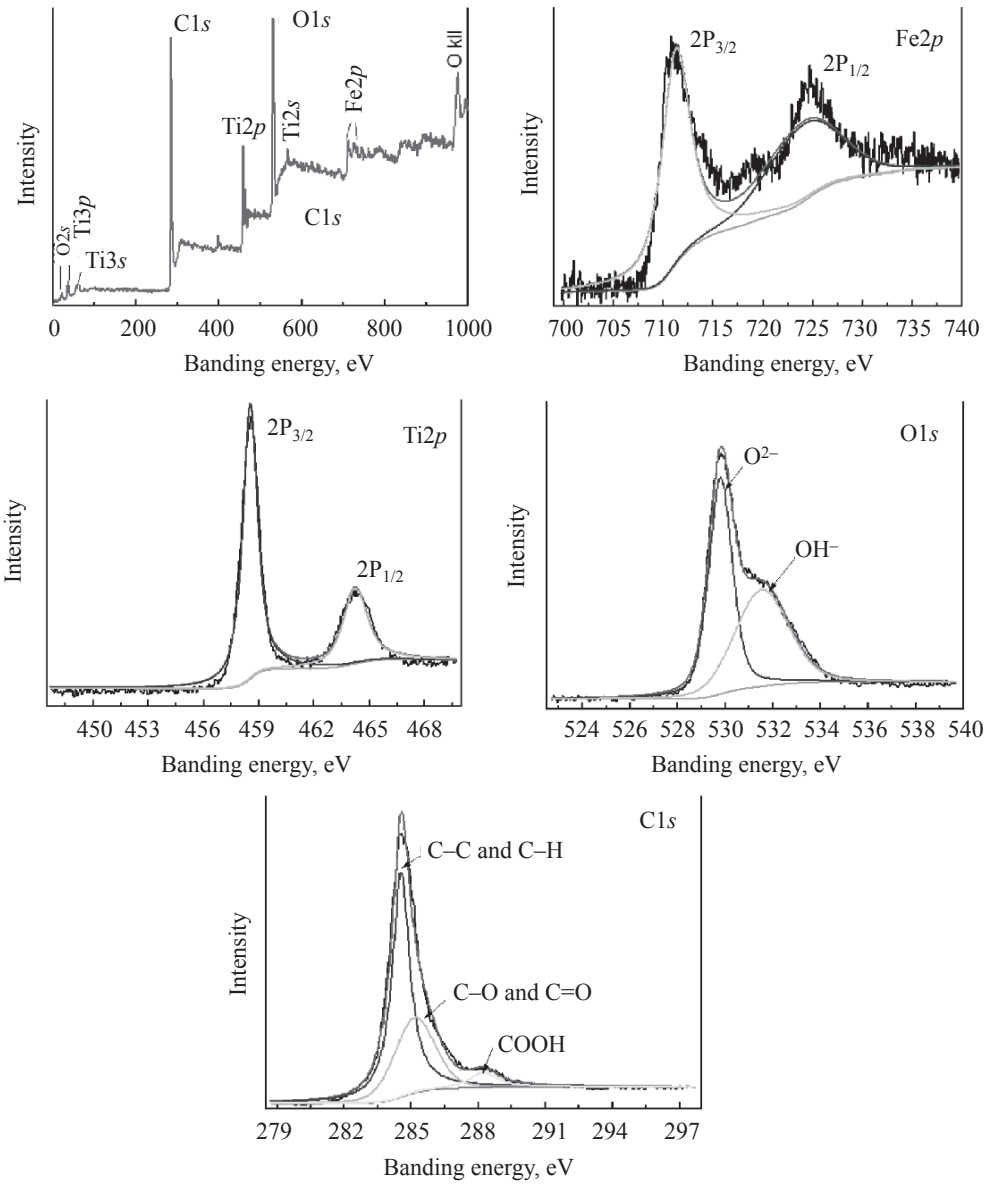

Fig. 5. General and characteristic elements XPS spectra of the sample calcined at 750°C for 5 h.

fibers have a porous structure and plenty of nano crystals are embedded in the m. From the elemental analysis, the elements of Ti, Fe, O and C are all detected in the composite fiber. Meanwhile, from the SAED pattern inset in the TEM image for the nano fibers, the (101), (004), (200) rings correspond well to that of anatase TiO_2, and the (110), (104), (116) rings correspond well to that of Fe_2O_3. Therefore, it can be identified that this nano fiber is composed of nano TiO_2, Fe_2O_3 and porous carbon fiber support.

The XPS spectra were recorded to establish the oxidation state and electronic environment of the elements present in the composite fibers. Figure 5 illustrates the XPS spectrum of Fe_2O_3−TiO_2@activated carbon fiber membrane and the XPS spectra of characteristic elements in high resolution, respectively. From the general XPS spectrum, the pattern indicates that the fiber surface contains all the expected elements such as Ti, Fe, O and C. Accordingly, from the spectra of individual lines of Ti2*p*, Fe2*p*, O1*s*, and C1*s*, the peaks at 464.3 eV and 458.6 eV belong to Ti2$p_{1/2}$ and Ti2$p_{3/2}$, respectively, which can been assigned to the Ti^{4+}. The peaks at 724.5 and 710.7 eV are due to Fe2$p_{3/2}$ and Fe2$p_{1/2}$, respectively, which can been

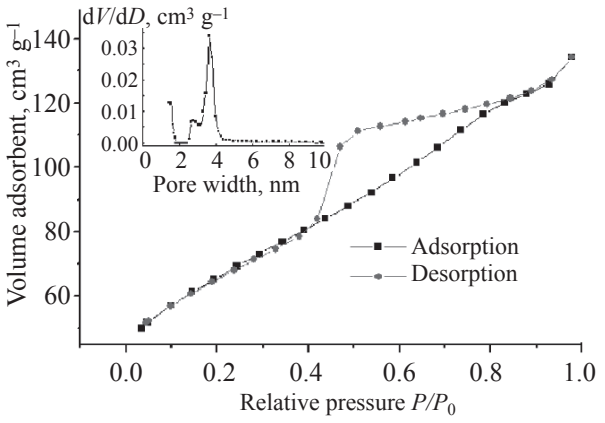

Fig. 6. Nitrogen adsorption/desorption isotherms of the sample calcined at 750°C for 5 h.

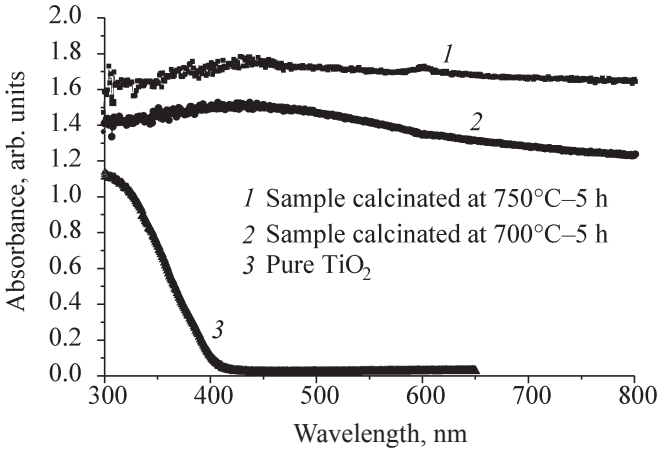

Fig. 7. UV-vis DRS of the samples compared with pure TiO_2.

assigned to the Fe^{3+}. The peak at 529.5 eV is ascribed to O1*s* bonded to Ti and Fe. The peak at 531.6 eV belongs to the hydroxyl groups, which can be attributed to the reaction of adsorbed H_2O with TiO_2 and formation of Ti–OH [28]. The C1*s* spectrum has been resolved into three individual component peaks. The first peak at 284.6 eV represents graphitic C–C and C Hn, the second one at 285.2 eV belongs to C–O groups and C=O groups, and the third one at 288.2 eV is due to COOH groups, which are well in agreement with the reported results [29].

Nitrogen adsorption/desorption isotherms of the Fe_2O_3−TiO_2@activated carbon fiber membrane (750°C for 5 h) are depicted in Fig. 6. It can be seen that the isotherms is due to type IV isotherms [30]. More definitely, the behavior of the adsorption/desorption isotherms can be regarded as a combination of the H3 loop subclass and H2 loop subclass of type IV isotherms since it does not exhibit any limiting adsorption at high P/P_0 values at 0.8–1.0, while evidently shows a hysteresis loop at medium P/P_0 values at 0.4–0.8, which are associated with capillary condensation in slit-like pores and irregular mesopores, respectively. The initial part of type IV isotherms can be attributed to monolayer- multilayer adsorption. Meanwhile, according to the isotherms, the BET specific surface area is up to 231.2 $m^2\ g^{-1}$, and the total pore volume amounts to 0.182 $cm^3\ g^{-1}$ calculated by the density function theory (DFT) method. The pore size distribution of the Fe_2O_3−TiO_2@activated carbon fiber shown in the inset figure is in the region from 2.4 nm up to 6 nm with a maximum pore volume at 3.7 nm. All these structural characteristics imply that the Fe_2O_3–TiO_2/activated carbon fiber membrane could have high adsorptive property.

Figure 7 shows the UV–vis diffuse reflectance spectra (DRS) of the fiber membrane calcinated at 700°C for 5 h and 750°C for 5 h, together with the pure anatase TiO_2 for comparison. Thereinto, the XRD for the sample calcined at 700°C for 5 h just displays a carbon peak, thus, the DRS of the sample at 700°C for 5 h can be mainly regarded as the contribution of carbon fiber. From Fig. 7, it can be observed that compared with the sample at 700°C for 5 h and pure TiO_2, the Fe_2O_3−TiO_2 activated carbon fiber membrane calcined at 750°C for 5 h exhibits stronger absorption not only in the ultraviolet region below 400 nm, but also in the visible light region at 400 –800 nm, and their absorption edge extents to a longer wavelength region, which is attributed to the c ombination of TiO_2 for ultraviolet light absorption with carbon and Fe_2O_3 for visible light absorption [25, 26]. This visible light excitable composite fiber membrane will greatly enhance the utilization efficiency of sunlight.

From the above characterization and analysis, this mesoporous nano Fe_2O_3−TiO_2@activated carbon fiber membrane not only has a visible light excitable photocatalytic activity, but also can be utilized as a adsorbent. Thus, the removal property of the fiber membrane for treating waste water was assessed by filtrating phenol solution under simulated visible light as described in Experimental part. Figure 8 is the UV-Vis adsorption spectra of phenol solutions w ith different cycles. It can be seen that the treated phenol solution after free penetration and irradiation has not revealed any

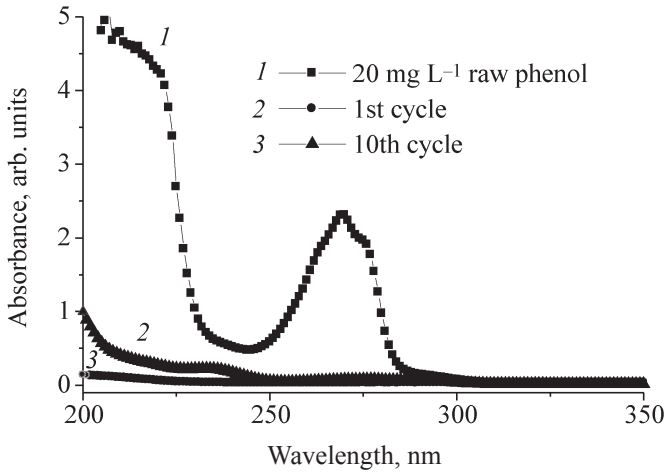

Fig. 8. UV-Vis adsorption spectra of phenol solutions with different cycles.

characteristic absorption peaks, meaning that the removal effic iency is nearly up to 100%. Furthermore, just a weak absorption below 250 nm occurs, possibly due to some undegraded intermediate products after 10th cycles.

CONCLUSIONS

The mesoporous nano-Fe_2O_3–TiO_2/activated carbon fiber membrane with a specific surface area of 231 $m^2 g^{-1}$ and narrow pore size distribution of 2.4–6 nm was prepared by an electrospinning method. This composite fiber membrane is not only a reusable adsorbent, but also a high efficient photocatalyst which has high photon absorption from both ultraviolet and visible lights. It can be used to remove phenol from waste water with a removal efficiency of 100%, and this technique is hopeful to be widely utilized in the treatment of various organic waste waters.

ACKNOWLEDGMENTS

This work was supported by National Natural Science Foundation of China (grant no. 51474113), the Science and Technology Support Program of Jiangsu Province of China (grant no. BE2013071), the Natural Science Research Program of Jiangs u Province Higher Education of China (grant no. 14KJB430010), and the Jiangsu Province's Postgraduate Cultivation and Innovation Project of China (SJZZ15-0131), and also thank the sponsorship of Jiangsu Overseas Research & Training Program for University Young &Middle-aged Teachers and Presidents.

REFERENCES

1. Gerdes, R., Wöhrle, D., Spiller, W., Schneider, J., Schnurpfeil, G., and Schulz-Ekloff, G., *J. Photochem. Photobiol. A: Chem.*, 1997, vol. 111, pp. 65–74.
2. Kahru, A., Maloverjan, A., Sillak, H., and Põllumaa, L., *Environ Sci. Pollut. Res. Int*., 2002, no. 1, pp. 27–33.
3. Kulkarni, S.J. and Kaware, J.P., *J. Sci. Res. Publications*, 2013, vol. 4, pp. 1–5
4. Gondal, M.A., Sayeed, M.N., and Alarfaj, A., *Chem. Physics Lett.*, 2007, pp. 445, pp. 325–330.
5. Meng, N.I., Michael, K.H., Leung, Denn, Y.C, et al., *Renew Able & Sust. Energy Revs*., 2007, vol. 11, pp. 401–425.
6. Schneider, J., Matsuoka, M., Takeuchi, M., Zhang, J., Horiuchi, Yu, Anpo, M., and Bahnemann, D.W., *Chem. Rev.*, 2014, vol. 114, no. 19, pp. 9919–9986.
7. Mya Mya Khin, A., Sreekumaran Nair, V., Jagadeesh Babu, Rajendiran Murugan, and Seeram Ramakrishna, *Energy Env. Iron. Sci.,* 2012, vol. 5, pp. 8075–8109.
8. Choi, Y., Kim, H., Moon, G., Jo, S., and Choi, W., *ACS Catalysis*, 2016, vol. 6, no. 2, pp. 821–828.
9. Liu, L., Chen, F., Yang, F., Chen, Y., and Crittenden, J., *Chem. Eng. J.,* 2012, pp. 181–182, pp. 189–195**.**
10. Dong-Min Yun, Hyun- Hee Cho, Jun-Won Jang , and Jae-Woo Park, *Water Res*., 2013, vol. 47, pp. 1858–1866.
11. Hongtao, Cui, Yan, Liu, and Wanzhong, Ren, *Adv. Powder Tech.,* 2013, vol. 24, pp. 93–97.
12. Juan Xie, Zhao Zhou, Yiwei Lian, Yong jing Hao, Pan Li, and Yu Wei, *Ceramics Int.*, 2015, vol. 41, pp. 2622–2625.
13. Patra, A.K., Dutta, A., and Bhaumik, A., *ACS Appl. Mater. Interfaces*, 2012, vol. 4, pp. 5022–5028.
14. Sun, P., Cai, Y., Du, S., Xu, X., Lu You, Ma, J., Liu, F., Liang, X., Sun, X., and Lu, G., *Sensors & Actuators B: Chem*., 2013, vol. 182, pp. 336–343.
15. Liu, J., Yang, S., Wu, W., Tian, Q., Cui, S., Dai, Zh., Ren, F., Xiao, X., and Jiang, Ch., *ACS Sustainable Chem. Eng.,* 2015, vol. 3, pp. 2975–2984.
16. Yao, K., Basnet, P., Sessions, H., Larsen, Simona, G.K., Hunyadi Murph, V., and Zhao, Y., *Catal. Today,* 2015. http://dx.doi.org/10.1016/j.cattod.2015.10.026.
17. Chen, M., Shen, X., Wu, Q., Li, W., and Diao, G., *J. Mater. Sci.,* 2015, vol. 50, pp. 4083–4094.
18. Zhang, X., Xie, Y., Chen, H., Guo, J., Meng, A., and Li, C., *Appl. Sur. Sci.*, 2014, vol. 317, pp. 43–48.
19. Liu, R. and Ou, H.T., *J. Nanotech.,* 2015, 727210.
20. Ibhadon, A.O. and Fitzpatrick, P., *Catalysts*, 2013, vol. 3,

pp. 189–218.

21. Suzuki, M., *Carbon*, 1994, vol. 32, pp. 577–586.
22. Brasquet, C. and Le Cloirec, P., *Carbon*, 1997, vol. 35, pp. 1307–1313.
23. Lee, K.J., Shiratori, N., Lee, G.H., Miyawaki, J., Mochida, I., Yoon, S., and Jang, J., *Carbon*, 2010, vol. 48, pp. 4248–4255.
24. Zhao, D., Yu, Y., and Chen, J.P., *RSC Adv.,* 2016, vol. 6, pp. 27020–27030.
25. Meng, H., Hou, W., Xu, X., Xu, J.,and Zhang, X., *Particuology,* 2014, vol. 14, pp. 38–43.
26. Shi, Jian-Wen, Cui, Hao-Jie, Chen, Jian-Wei, Fu, Ming-Lai, Xu, Bin, Luo, Hong-Yuan, Ye, and Zhi-Long, *J. Colloid & Int. Sci.*, 2012, vol. 388, pp. 201–208.
27. Hurum, D.C., Agrios, A.G., and Gray, K.A., *Phys. Chem. B*, 2003, vol. 107, no. 19, pp. 4545–4549.
28. Fu, P., Luan, Y., and Dai, X., *J. Mol. Catal. A: Chem.*, 2004, vol. 221, pp. 81–88.
29. Palanisamy, B., Babu, C.M., Sundaravel, B., Anandan, S., and Murugesan, V., *J. Hazardous Mat.,* 2013, pp. 233–242.
30. Aboul-Gheit, A.K., El-Desouki, D.S., and El-Salamony, R.A., *Egypt. J. Petroleum,* 2014, vol. 23, pp. 339–348.